Electronic Supplementary Material (ESI) for Energy & Environmental Science.
This journal is © The Royal Society of Chemistry 2022

Supplementary Information

A strongly complexed solid polymer electrolyte enables stable solid state high-voltage lithium metal battery

*Hangchao Wang,[a] Jin Song,[a] Kun Zhang,[a] Qiu Fang,[b] Yuxuan Zuo,[a] Tonghuan Yang,[a] Yali Yang,[a] Chuan Gao,[a] Xuefeng Wang,[bc] Quanquan Pang[a] and Dingguo Xia[a]**

*Corresponding author. Email: dgxia@pku.edu.cn

a. Beijing Key Laboratory of Theory and Technology for Advanced Batteries Materials, School of Materials Science and Engineering, Peking University, Beijing 100871, PR China. E-mail: dgxia@pku.edu.cn.

b. Laboratory for Advanced Materials & Electron Microscopy, Institute of Physics, Chinese Academy of Sciences, Beijing 100190, China; College of Materials Science and Opto-Electronic Technology, University of Chinese Academy of Sciences, Beijing 100049, China

c. Tianmu Lake Institute of Advanced Energy Storage Technologies Co. Ltd., Liyang, 213300, Jiangsu, China.

Materials and methods

Synthesis of the UPyMA monomer

The monomer was synthesized based on the methods described in previous work [1]. First, 1.5 g of 6-methylisocytosine (Sigma-Aldrich; 99%) was added into 27.5 mL of dimethyl sulfoxide (DMSO, Sigma-Aldrich; AR), and stirred for 10 min at 150°C. Then the solution was cooled to ambient temperature and 1.98 g of 2-isocyanatoethyl methacrylate (Sigma-Aldrich; 98%) was added to the flask, which precipitated a white solid when the mixture was cooled using an ice bath. Then, the precipitate was collected and washed several times with methanol and acetone to remove the residual DMSO. Afterward, the precipitate was dried under a vacuum at 30°C for 4 h, and the obtained white powder was collected.

Preparation of the ASPE electrolyte

To prepare the DES electrolyte, lithium bis(tri-fuoromethanesulfonyl)imide (LiTFSI, Aladdin; 99%, dried at 100°C for 12 h in a vacuum before use) and N-methylurea (NML, Sigma-Aldrich; 99%, dried at 35°C for 24 h in a vacuum before use) were mixed at different molar ratios at 55°C until a transparent solution was obtained. Then, the UPyMA monomer was dissolved in the DES electrolyte, and then the mixture was heated to 55°C until it became transparent. Afterward, poly(ethylene glycol) diacrylate (PEGDA, MW 600, 99%, Aladdin) (EO: Li^+=20:1) as the polymer electrolyte body and 0.2 wt% 2,2′ azobis(2-methylpropionitrile) (AIBN) as the initiator were added to the mixture, obtaining a transparent precursor solution. Then, the polymerization was thermally initiated at 70°C for 20 min to obtain the ASPE electrolyte. Solid-state polymer electrolyte preparation and cell assembly were conducted in an argon gas filled glove box (inert), in which both O_2 and H_2O content were maintained below 0.1 ppm.

The polymer matrix was separated from the ASPE electrolyte by washing with acetone, then the mixture was centrifuged at 8000 rpm for 10 min. The above procedures were repeated five times, and the white precipitate was vacuum-dried at 80°C to obtain the separated PEGDA-UPyMA copolymer matrix.

Preparation of other solid electrolytes

ASPE without NML: The UPyMA monomer and LiTFSI were dissolved in the liquid PEGDA (EO: Li^+=20:1), and then the mixture was heated to 55°C until it became transparent. Afterward, 0.2 wt% AIBN as the initiator were added to the mixture, obtaining a transparent precursor solution. Then, the polymerization was thermally initiated at 70°C for 20 min to obtain the ASPE without NML electrolyte.

PEGDA@DES: To prepare the DES electrolyte, LiTFSI and NMLwere mixed at 55°C until a transparent solution was obtained. Then, the PEGDA (EO: Li^+=20:1) as the polymer electrolyte body and 0.2 wt% AIBN as the initiator were added to the mixture, obtaining a transparent precursor solution. Then, the polymerization was thermally initiated at 70°C for 20 min to obtain the PEGDA@DES electrolyte.

PEGDA without NML (PEGDA electrolyte): The LiTFSI was dissolved in the liquid PEGDA (EO: Li^+=20:1), and 0.2 wt% AIBN as the initiator were added to the mixture, obtaining a transparent precursor solution. Then, the polymerization was thermally initiated at 70°C for 20 min to obtain the PEGDA without NML (PEGDA electrolyte).

Cathode and battery preparation

The cathode ($LiCoO_2$, $LiFePO_4$, and $Li_{1.2}Ni_{0.13}Co_{0.13}Mn_{0.54}O_2$) was prepared using a simple coating method. The cathode electrode was prepared by mixing the cathode materials (solid-state cell active material, 75wt%; liquid electrolytes of the battery's active material, 80%), conductive carbon black (super-P, 10 wt%), poly(vinylidene fluoride) (10 wt%), and polymer electrolyte precursor solution (5 wt%) in anhydrous N-methyl-2-pyrrolidone (NMP). Then, the homogeneous cathode slurry was cast on Al foil. Afterward, the electrode was dried under a vacuum at 110°C for 12 h, where the typical mass loading of the active materials was 2.5 mg cm^{-2}. Coin 2032-type cells were assembled using a cathode, liquid electrolyte (40 µl) or ASPE, and lithium metal inside an argon filled Glovebox. The coin cells were assembled using Li foil as the anode and used glass fiber for the $Li_{1.2}Ni_{0.13}Co_{0.13}Mn_{0.54}O_2$ half cell as the separator, and Celgard for the $LiCoO_2$ or $LiFePO_4$ half cells as the separator. Then, precursor solution electrolyte was injected into the cells. The separator was used for the assembly of the cells, to provide separation and control the

thickness of the solid polymer electrolyte; thus, preventing a short circuit in the liquid state. The assembled cathode materials//Li cells were aged for 2.5 h, and subsequently, the cells were heated for 20 min at 70°C to ensure complete polymerization.

The rate capability and cycle life of the Li | electrolytes | $LiCoO_2$, Li | electrolytes | $LiFePO_4$, and Li | electrolytes | $Li_{1.2}Ni_{0.13}Co_{0.13}Mn_{0.54}O_2$ half cells were measured on a Neware testing system (ShengZhen, Neware Electronics Co., Ltd.) at voltage ranges of 3.0~4.6 V (LCO), 1.8~4.2 V (LFP), and 2.1~4.9 V (LNCM) at ambient temperature. The C rates of all electrochemical measurements were defined on the basis of 1 C = 180, 1 C = 170, and 1 C = 250 mA g^{-1}. All electrochemical cell performances were tested at room temperature. Here in our work, we use a lithium metal foil of 20 μm thickness and a $LiCoO_2$ cathodes of 25 mg cm^{-2}, and this leads to a N/P ratio of 0.993; but as we have full amount of lithium in the $LiCoO_2$ cathode, the actual N/P ratio here is 1.993, meaning 99.3% excess of lithium. Regarding the coin cells, large excess of lithium metal is used as the counter electrode so that it is considered as Li-metal half cells.

Material characterization

The FTIR spectra were recorded using a Thermo Nicolet AVATAR 360 infrared instrument employing the attenuated total reflectance technique with wavenumbers from 3000 to 500 cm^{-1}. The Raman spectra were obtained by a LabRAM HR Evolution spectrometer from 600 to 1000 cm^{-1}. The microstructure and morphology of the Li metal, LCO, and polymer electrolyte membranes were examined by a Zeiss SUPRA-55 scanning electron microscope with an accelerating voltage of 15 kV, while the XRD spectra were measured using an automated multipurpose X-ray diffractometer (Smartlab) with Cu Kα radiation (λ = 1.5418 Å). The equipment was operated at a voltage of 45 kV, an electrical current of 200 mA, and a scan rate of 5°/min. The ^1H nuclear magnetic resonance (NMR) spectra were measured on an Agilent 500 MHz NMR spectrometer with $CDCl_3$ as the solvent under ambient temperature. DSC was used to measure the phase transition temperature of the polymer using a Q2000 calorimeter (TA Instruments Inc.) under a nitrogen atmosphere with a heating rate of 10°C/min at a temperature range of −70 to 100°C. The thermal properties of the prepared solid polymer electrolytes were characterized by thermogravimetric analysis on Perkin Elmer equipment at a heating rate of 10°C/min in the range of 30–600°C. A tensile testing machine was used to obtain the stress-strain curves of the solid polymer electrolytes with a tensile speed of 0.2 cm/min. The rheological measurements were performed using oscillatory shear rheology (ARES-LS rheometer) with parallel-plate geometry (diameter of 10 mm). The oscillatory shear experiments were carried out at a strain of γ = 2% and

a shear rate of ω = 0.1~100 rad/s was used at ambient temperature. The XPS experiments were carried out on a high-resolution Kratos AXIS 165 X-ray photoelectron spectrometer using monochromic Al Kα radiation. The cycled Li and LCO were adequately washed with dimethoxyethane and dried in the glove box. The synchrotron radiation small angle X-ray scattering (SAXS) patterns were obtained at BL16B1 beamline, SSRF (energy ring 3.5 GeV, beam current 220 mA). The X-ray wavelength was 0.12398 nm with a spot size of 1 mm^2, and the sample-to-detector distance was 1900 mm. A Pilatus3S2M detector was also used to collect the SAXS patterns. The high-resolution images were obtained on JEOL JEM-F200 microscope at 200 KV. TEM grid was loaded on a cryo vacuum-transfer holder (Fischione 2550) in an argon-filled glove box and transfered to TEM chamber without air exposure. The sample was maintained at cryogenic temperature (-180^{o}C) during the whole experiment. AFM (Bruker–Fastscan) experiment was operated in a dry room environment.Scan rage: XY maximum scanning range: 90 μm × 90 μm, Z ≤ 3 μm.

Electrochemical measurements

The electrolyte membranes were sandwiched between two stainless steel (SS) electrodes at a diameter of 16 mm, and the coin cells (CR2032) of SS| electrolytes |SS were assembled to determine the ionic conductivity values. Electrochemical impedance spectroscopy (EIS) was conducted using a CHI 660E electrochemical workstation (Shanghai Chenhua Instrument Co., Ltd.) at a temperature range of 25°C to 70°C, where the frequency range was set from 0.1 Hz to 1 MHz with an amplitude of 10 mV. The ionic conductivity values were obtained by the following equation:

$$\sigma = L/(S*R),$$

where L (cm) is the thickness of the ASPE membrane (about 60 μm and measured by the micrometer), R (Ω) is the bulk resistance of the electrolyte obtained from EIS, and S (cm^2) denotes the contact areas of the electrode and electrolyte. The electrochemical stability windows of the solid polymer electrolytes were determined by linear sweep voltammograms (LSV) from 0 to 7 V at a scan rate of 1 mV/s using Li| electrolytes |SS. The lithium-ion transference numbers (t_{Li+}) of the solid polymer electrolytes were tested according to the methods proposed by Abraham et al. The Li| electrolytes |Li symmetrical cells were assembled and subjected to EIS measurements

combined with the steady-state current technique. The lithium-ion transference number (t_{Li+}) was also obtained by the following equation:

$$t_{Li+} = I_S\,(\Delta V - I_0R_0)/I_0(\Delta V - I_SR_S).$$

The cell was polarized at 10 mV (ΔV) to determine the currents, including the initial (I0) and the steady state (IS), until the current was steady. Interfacial resistance was obtained from EIS before (R0) and after (RS) polarization, and the interfacial compatibility of the solid polymer electrolyte was measured by monitoring the interfacial resistance of the Li| electrolytes |Li cells at different cycles. Coulombic efficiencies of Li plating and stripping cycles were studied via a Li||Cu cell configuration. In each cycle, 1.5 mA h cm^{-2} of Li was plated on the Cu electrode at a current density of 1.0 mA cm^{-2}, and then stripped until the potential reached 0.5 V vs. Li/Li^+.

Fig. S1. Digital images of (**A**) LiTFSI (**B**) N-Methylurea (NML) and (**C**) DES.

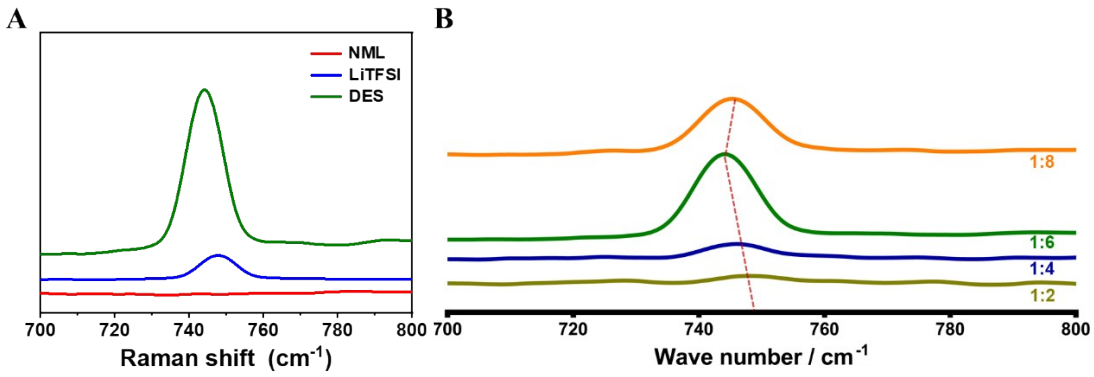

Fig. S2. Raman spectra of DES, NML, LiTFSI (**A**) and DES formed by different molar ratios of LiTFSI: NML (**B**). The stretching vibration characteristic peak of the anionic group in LiTFSI is located at 748cm^{-1}, and the characteristic peak appears at 745cm^{-1}after the interaction with amide. The molar ratio is 1:6 is nearly the eutectic point and can maintain the DES in the liquid state for a wider temperature range.

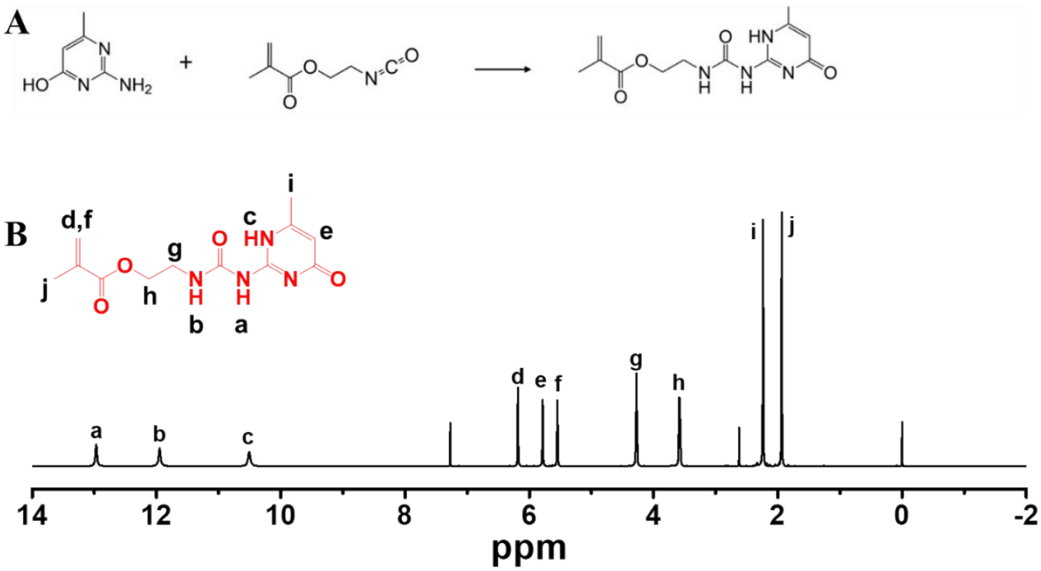

Fig. S3. Reaction route (**A**) to synthesize the UPyMA monomer from 6-methylisocytosine and 2-isocyanatoethyl methacrylate. (**B**)1H NMR spectrum of the prepared (2-(3-(6-methyl-4-oxo-1,4-dihydropyrimidin-2-yl)ureido)ethyl methacrylate) (UPyMA).

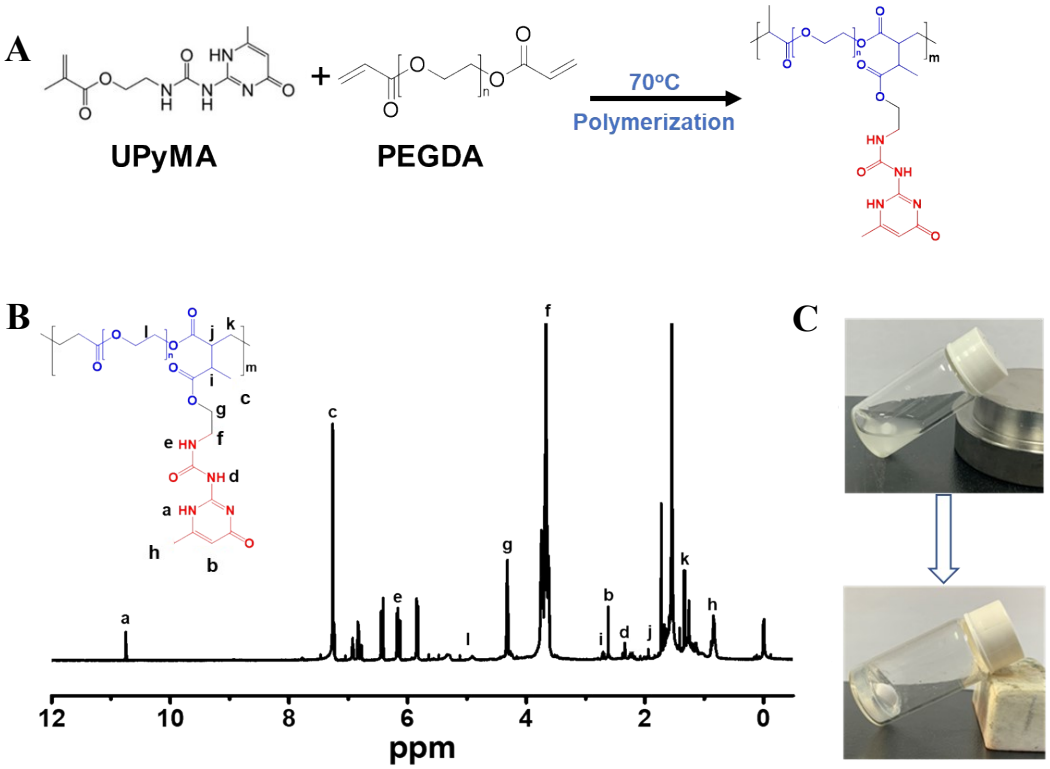

Fig. S4. Schematic illustration of (**A**) the synthesis of the polymer electrolyte body copolymer and (**B**)1H NMR spectrum of the polymer electrolyte body. (**C**) solid-state polymer electrolyte formed spontaneously.

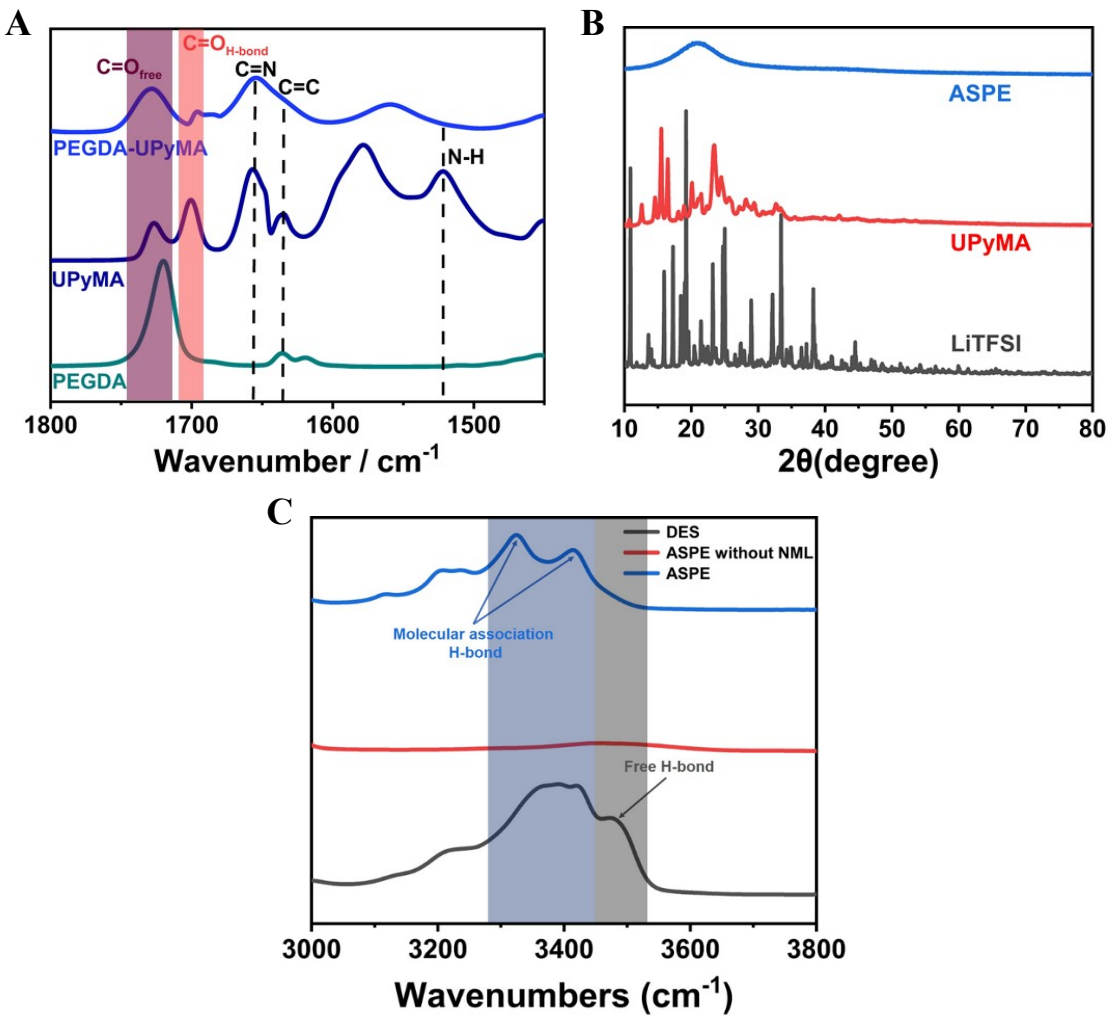

Fig. S5. (**A**) FT-IR spectra of PEGDA monomer, UPyMA monomer, and PEGDA-UPyMA. (**B**) XRD spectra of LiTFSI, UPyMA and ASPE, respectively. (**C**)Status of DES in pure DES and the ASPE electrolyte membrane analyzed by FTIR spectroscopy. The FTIR peak positions for free H-bond about 3480 cm^{-1}, respectively. The free DES (Free H-bond) in the solution almost disappears. When the ASPE electrolyte is formed, the coordination molecules (Molecular association H-bond) dominate.

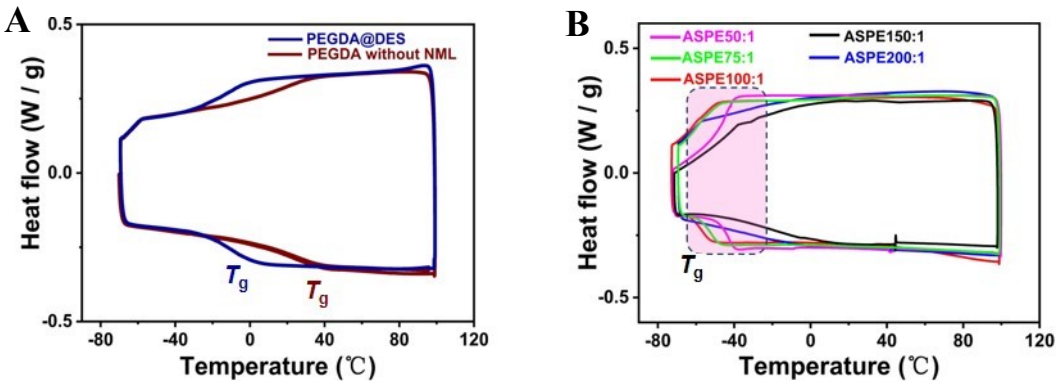

Fig. S6. **DSC traces characteristics of SPEs with different compositions. (**A) PEGDA@DES and PEGDA without NML electrolyte and (B) the SPEs with different concentrations of UPyMA. The presence of DES significantly reduces the T_g, which is consistent with the experimental results of the tested ionic conductivity, and as the UPy unit in the polymer increases, its Tg will also change regularly. This is because the UPyMA unit passes through the quadruple hydrogen bond. The interaction between the polymer chain molecules is changed, and the movement of the polymer chain segments is affected.

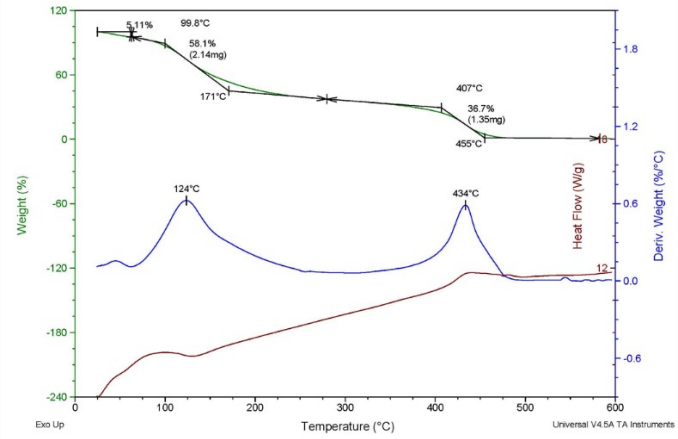

Fig. S7. **TGA thermograms of the DES.** The starting weight of sample is 3.6840 mg. Method: ramp10K / min N_2 100mL / min.

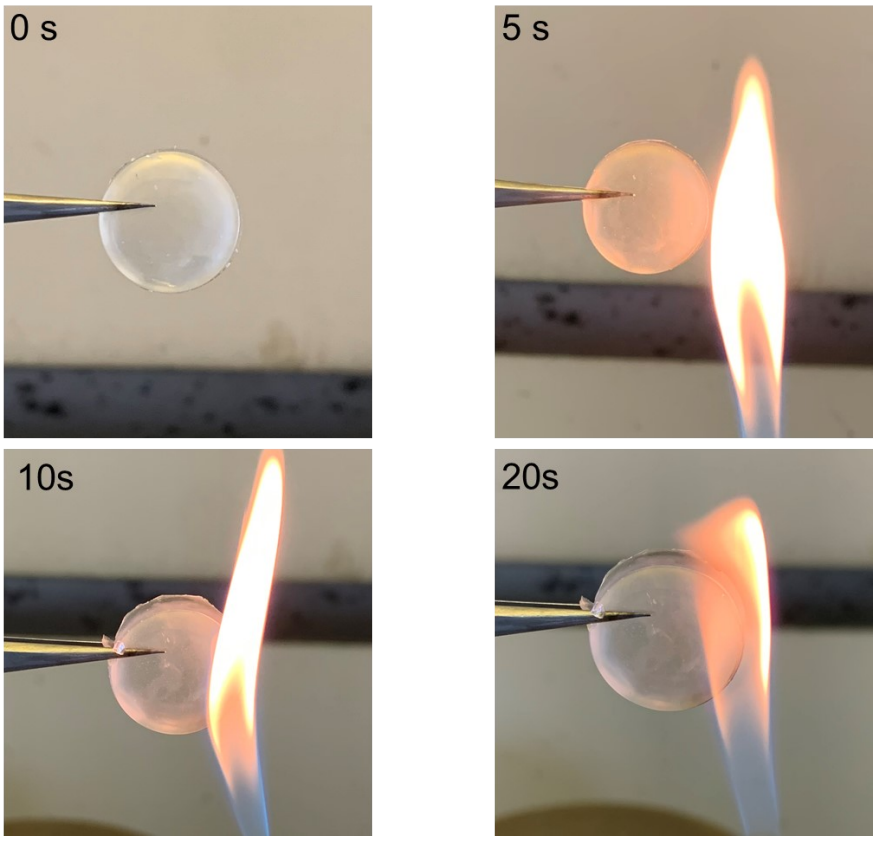

Fig. S8. **Optical images of SPE under a combustion test.** The ASPE electrolyte blend could not be ignited even more than 20s in the flame. It indicated that ASPE has a good flame retardant property, which improves the safety of the battery.

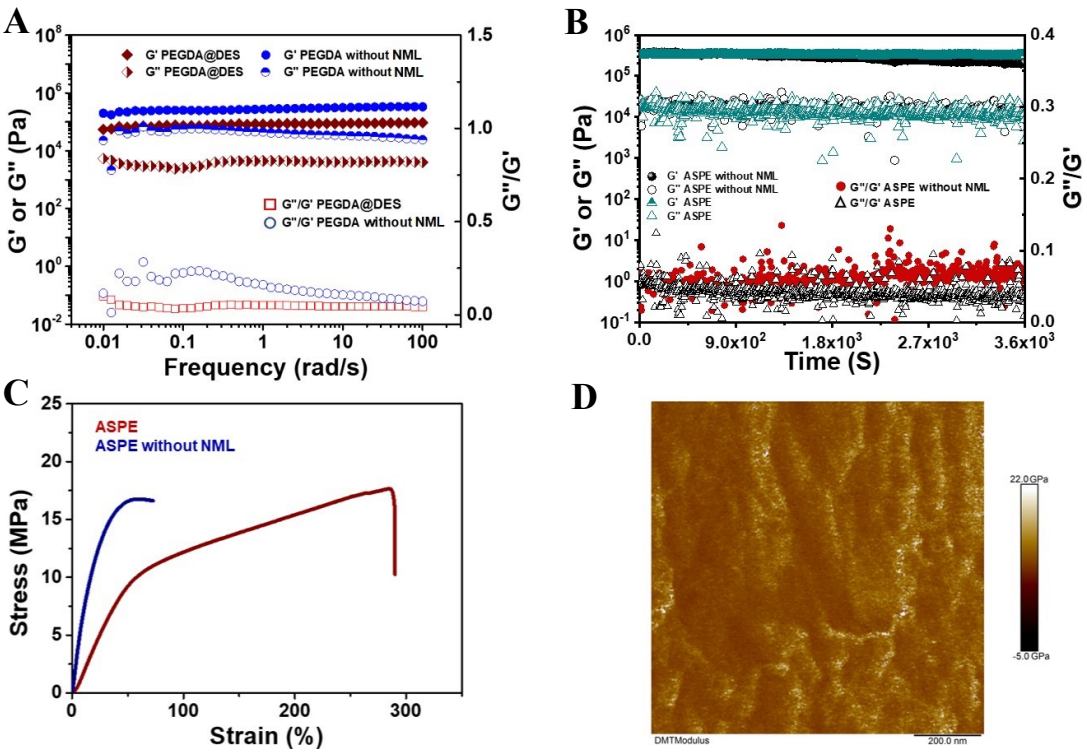

Fig. 9. **The dynamic mechanical properties of the prepared SPEs were also studied by small-amplitude oscillatory shear measurements (A), (B) and tensile analysis (C) and shear modulus of ASPE (D).** The storage modulus (G', compared with Fig. 2C) increases with the increase of UPyMA units in the polymers, indicating that the UPyMA units improved the intermolecular interaction of polymer chains via quadruple hydrogen bonding. Storage modulus dominates the loss modulus at all frequencies and time. This behavior is typical of materials in the dynamic universal class viscoelastic solids, it provides fundamental support for their classification as solid-state polymer electrolytes. The stress-strain curve result demonstrate that the SPE based on multiple hydrogen bonding networks is able to offer the SPE outstanding mechanical strength and stretchable capabilities, which are beneficial to extend the life time and to improve the safety of SPEs.

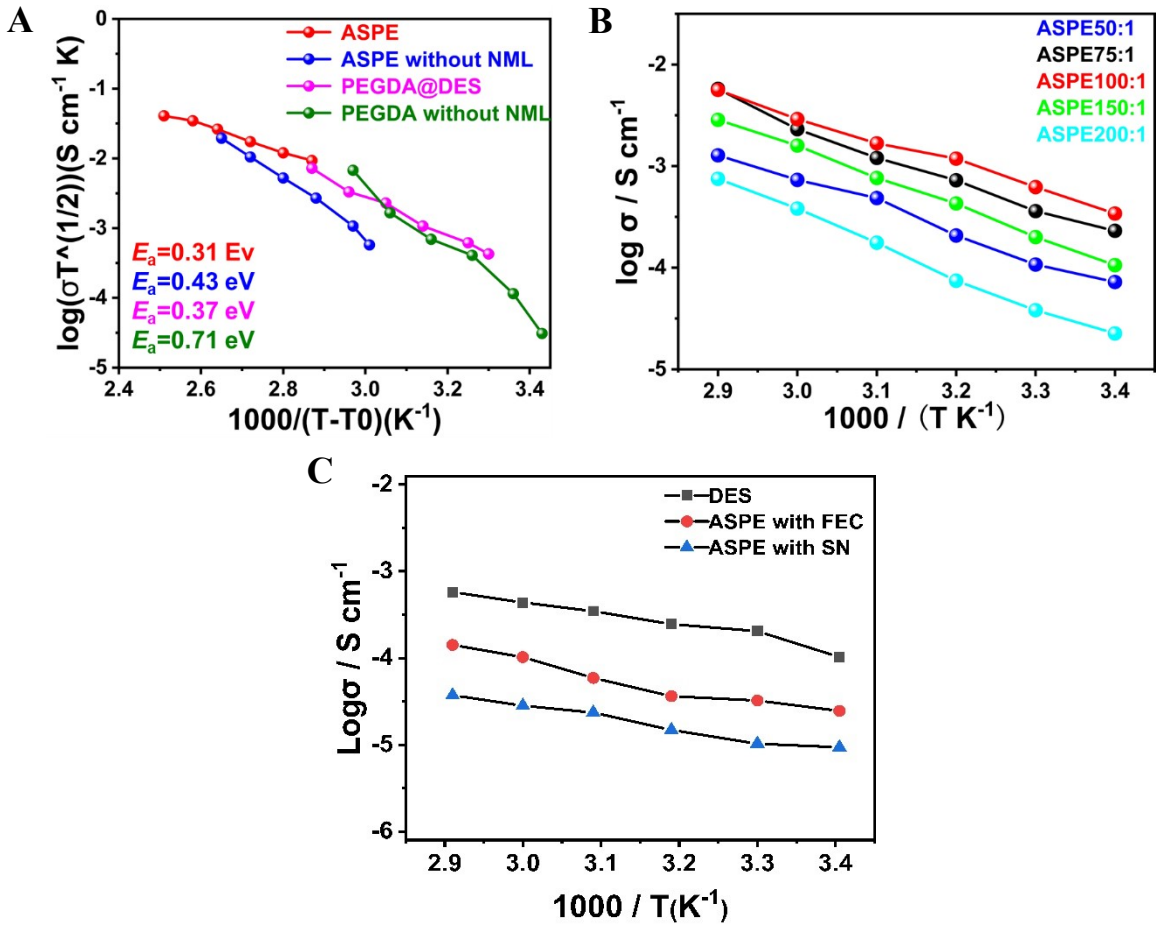

Fig. S10. (**A**) Vogel–Tammann–Fulcher (VTF) plot of different electrolytes at temperatures from 25°C to 70°C. The Vogel–Tammann–Fulcher (VTF) equation below: $\sigma = \sigma_0 T^{-\frac{1}{2}} \exp\left(-\frac{E_a}{R(T-T0)}\right)$ in which σ_0 is the pre-exponential factor, E_a is the activation energy, T_0 is the effective glass transition temperature, and R is the ideal gas constant. (**B**) Ionic conductivities as a function of temperature based on different PEGDA: UPyMA mass ratios**.** In the test temperature range, the mass ratio is 100:1 ASPE has the highest ionic conductivity. (**C**)Ionic conductivities of DES and ASPE with a common plasticizer as functions of temperature. To avoid short circuit in the liquid state, Celgrad is used as a separator (Thickness 25μm). Fluoroethylene carbonate (FEC) and succinonitrile (SN) were selected as common plasticizer for experimental comparison. In order to ensure the accuracy of the experiment, the percentage content of FEC and SN in the polymer electrolyte is consistent with that of NML in the polymer electrolyte, and remained the same in the following experiment.

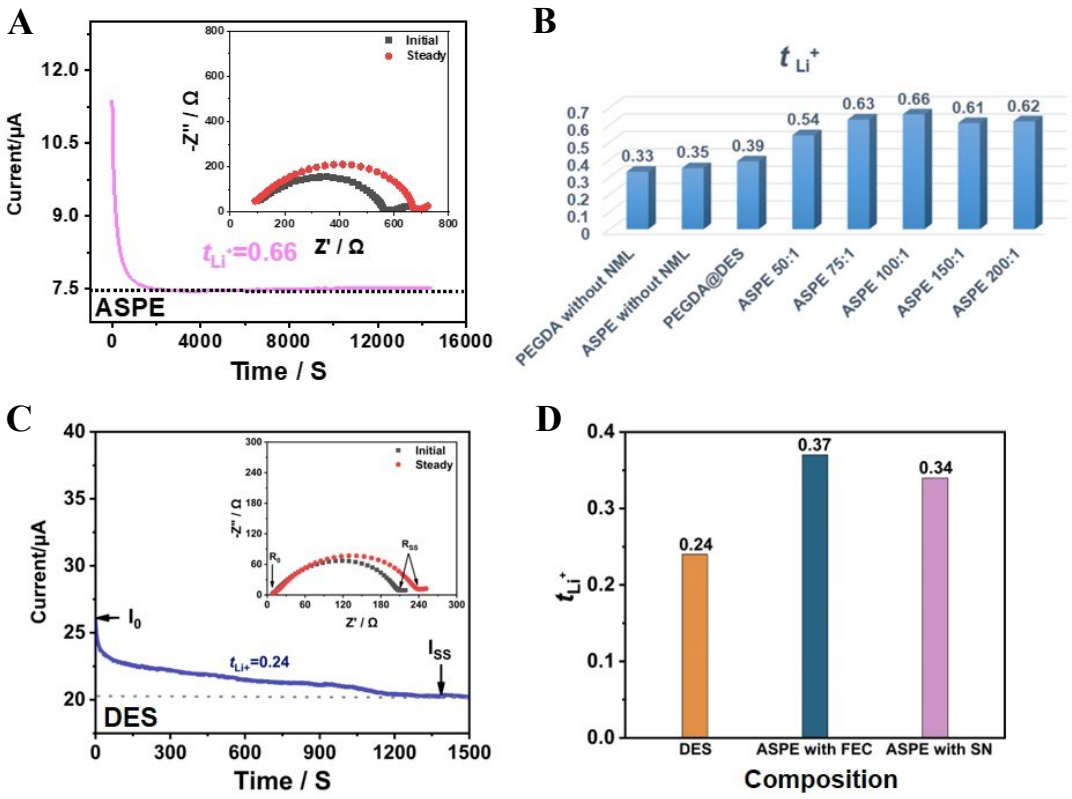

Fig. S11. **The lithium-ion transference number.** (**A**) Chronoamperometry profile of Li|ASPE|Li cells under 10 mV polarization voltage. Inset: Corresponding electrochemical impedance spectroscopy (EIS) profiles before and after polarization. (**B**) lithium-ion transference of different electrolytes tested with the above method. (**C**) Chronoamperometry profile of Li | DES | Li cells under 10 mV polarization voltage. Inset: Corresponding electrochemical impedance spectroscopy (EIS) profiles before and after polarization. (**D**) Lithium-ion transference of ASPE with a common plasticizers tested with the above method. Fluoroethylene carbonate (FEC) and succinonitrile (SN).

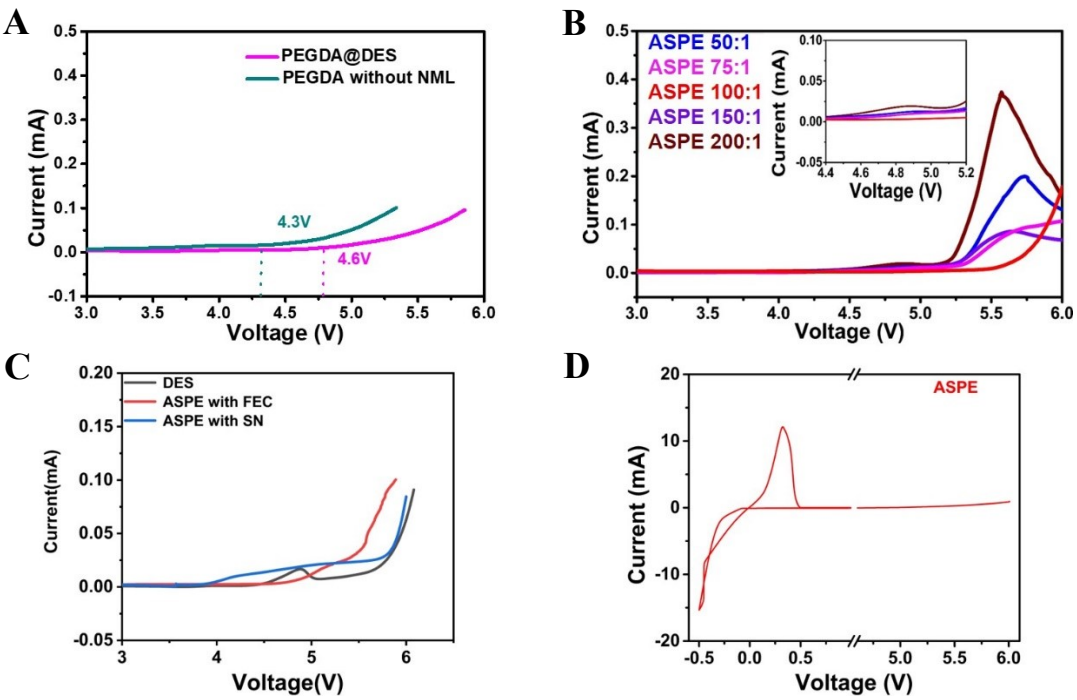

Fig. S12. (**A**) Linear sweep voltammetry PEGDA@DES and PEGDA without NML as a sweep rate of 1mV s^{-1}. The electrochemical stability window of polymer electrolytes without UPyMA are generally lower, which indicates that the quadruple hydrogen bond has a positive effect on the electrochemical stability, and the effect of van der Waals force can effectively broaden the electrochemical window. Similarly, the presence of DES widens PEGDA electrochemical stabilization window to 4.6 V. (**B**) Linear sweep voltammetry ASPE with different mass ratio of PEGDA and UPyMA as a sweep rate of 1mV/s. With the increase of UPyMA monomer, the electrochemical stability window of ASPE first increased and then decreased. Combined with Figure 3e, it can be concluded that the electrochemical window reached the highest when the mass ratio of PEGDA: UPyMA reached100:1. (**C**)Linear sweep voltammetry of DES、ASPE with FEC and ASPE with SN at a sweep rate of 1 mV/s. ASPE with SN electrolyte has the worst electrochemical stability, with an oxidation peak at about 3.9V, while DES electrolyte has an oxidation peak at about 4.4 V, and ASPE with FEC electrolyte has the best electrochemical stability, reaching 4.6V. (**D**) Cyclic voltammetry curves of Li|ASPE|SS cell from -0.5 to 6.0 V (sweep rate of 1 mV s^{-1}), showing ASPE have excellent stability to Li metal and good oxidation stability up to 5.0 V.

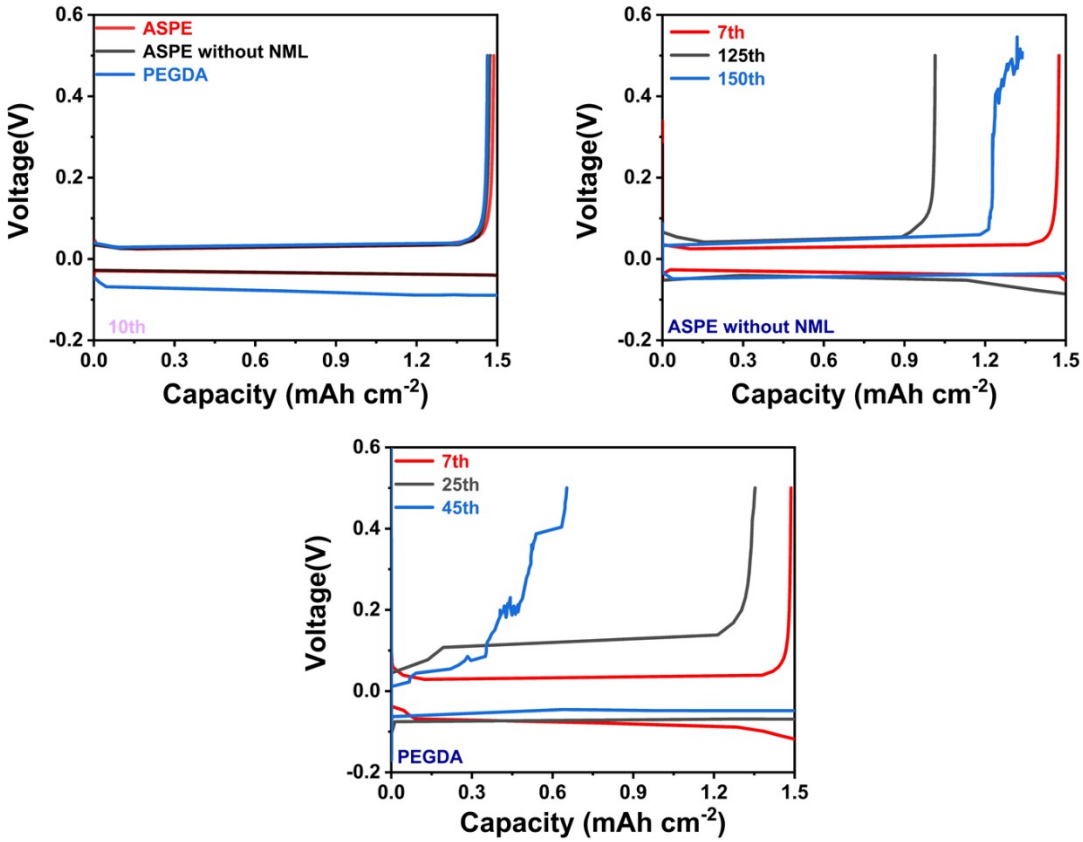

Fig. S13. Li stripping and plating properties of Li-Cu cells using different Electrolytes. The current density is 1 mA $cm^{-2}$and the plating Li capacity is 1.5mAh cm^{-2} per cycle.

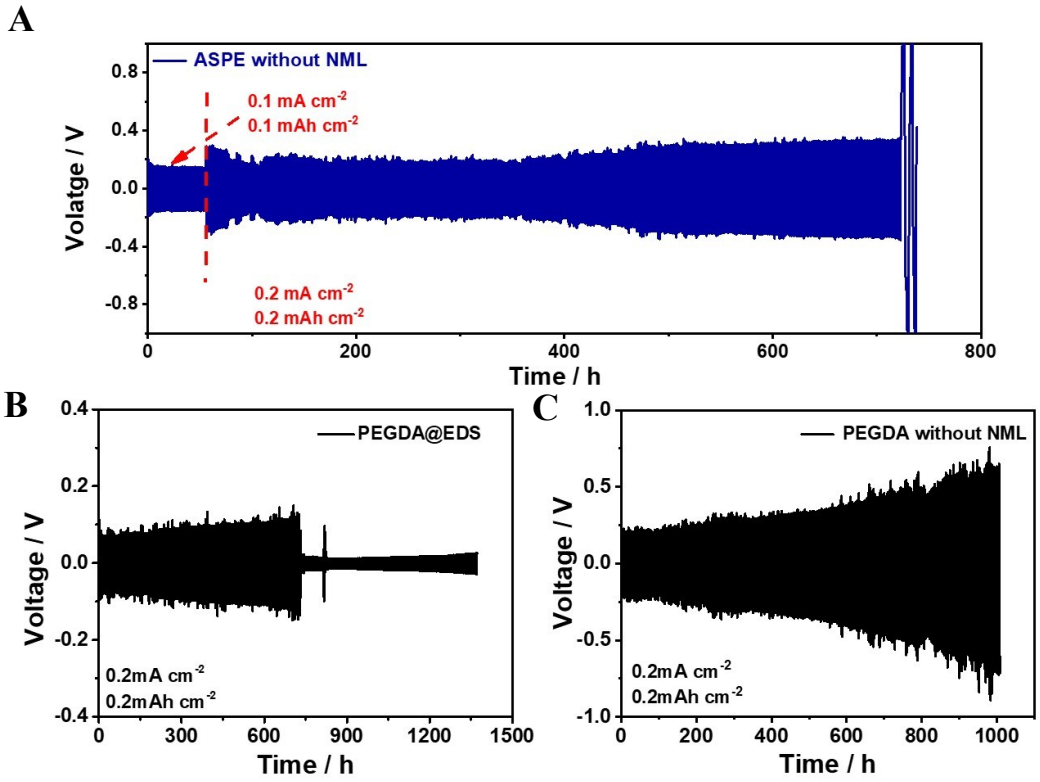

Fig. S14. Lithium plating/stripping experiment for symmetric Li||Li cells with different electrolytes at a current density of 0.2 mA cm^{-2}. (**A**) ASPE without NML; (**B**) PEGDA@DES; (**C**) PEGDA without NML. The polarization of Li|ASPE without NML|Li symmetric battery begins to increase at about 400 h, and the polarization of symmetrical battery increases sharply when the circuit is broken at 710h.The polarization of Li|PEGDA@DES|Li symmetric battery decreases suddenly in 700h, resulting in short circuit of electrolyte. Different from the above, the polarization of Li|PEGDA without NML|Li symmetric battery is increased throughout.

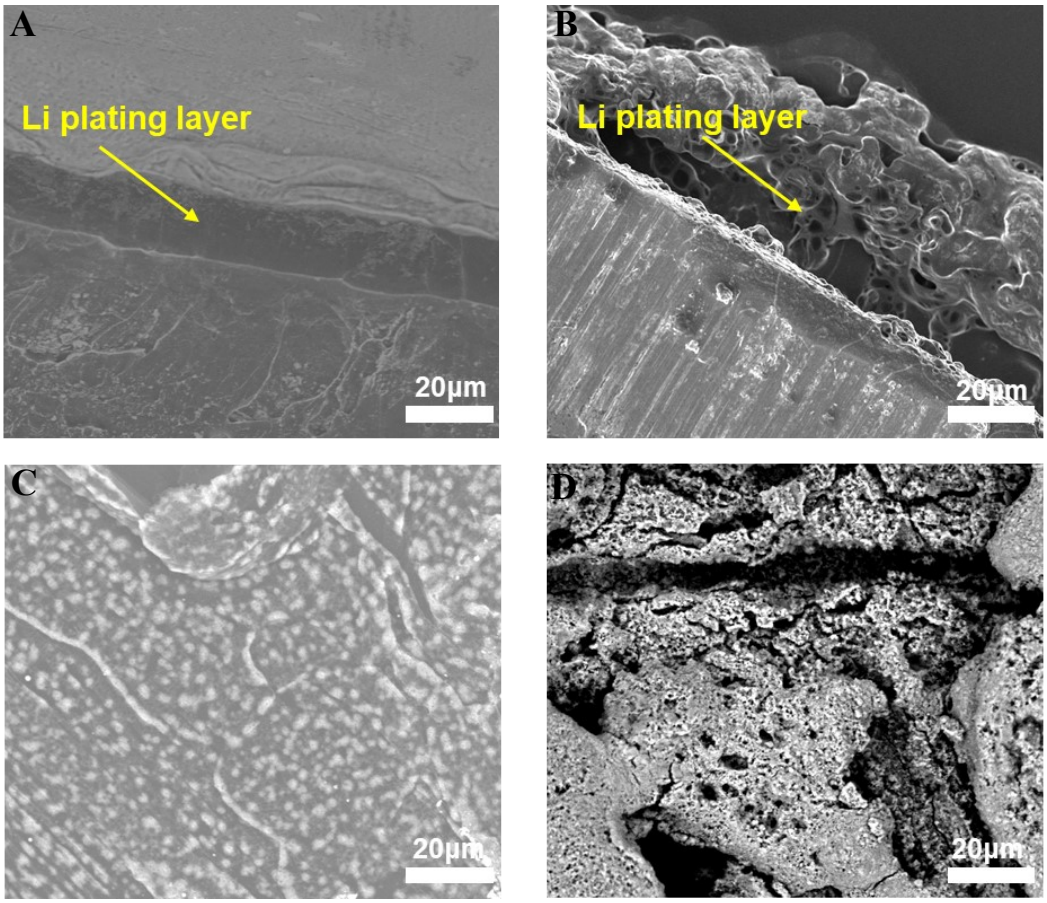

Fig. S15. SEM of interfacial Li deposition behavior. (**A** and **C**) Cross-sectional and surface SEM images of Li deposition layers (Li|ASPE|Li). (**B** and **D**) Cross-sectional and surface SEM images of the Li deposition layer (Li|PEGDA|Li). SEM of interfacial Li deposition behavior after 40 hour electrodeposition under a current density of 2 mA cm^{-2} (4 mAh cm^{-2}) in symmetric Li cell.

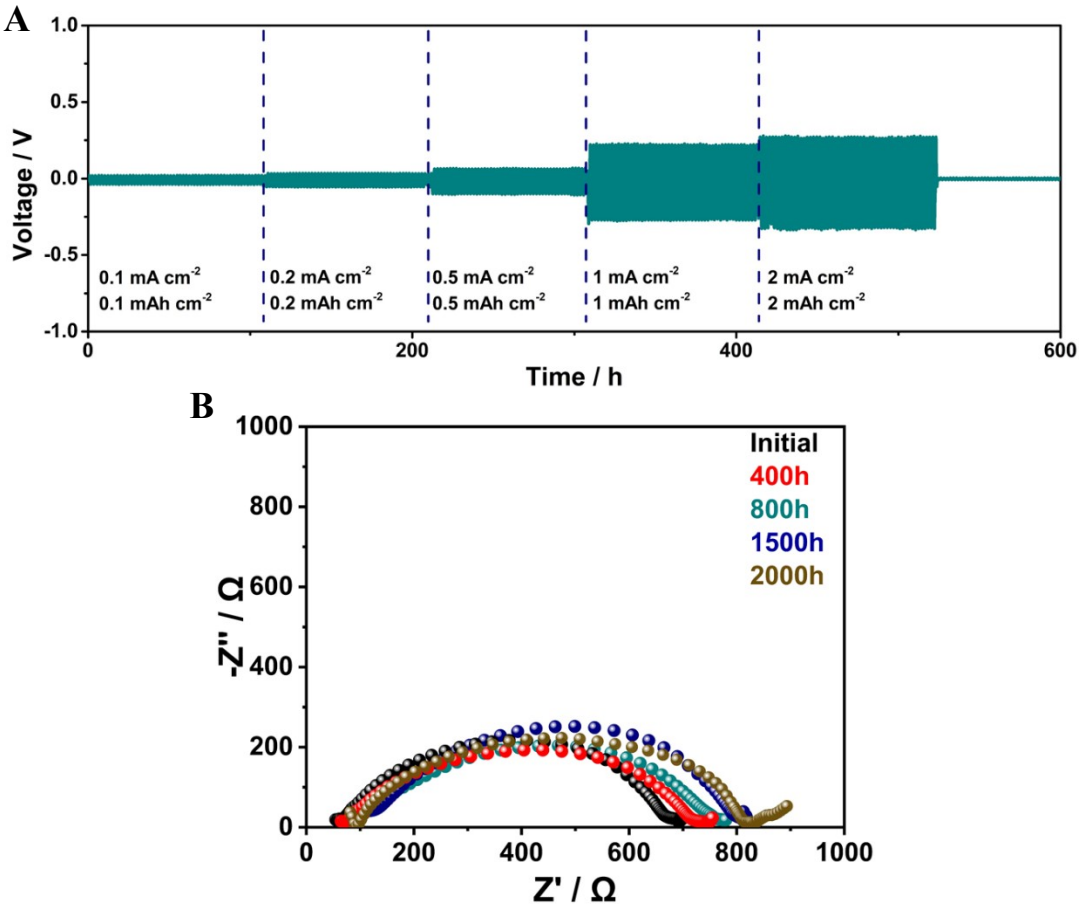

Fig. S16. (**A**) Li plating/stripping experiment featuring symmetric cells with ASPE at current densities of 0.1, 0.2, 0.5, 1.0, and 2.0 mA cm^{-2}. (**B**) Alternating current impedance profiles of Li|ASPE|Li at different cycles.

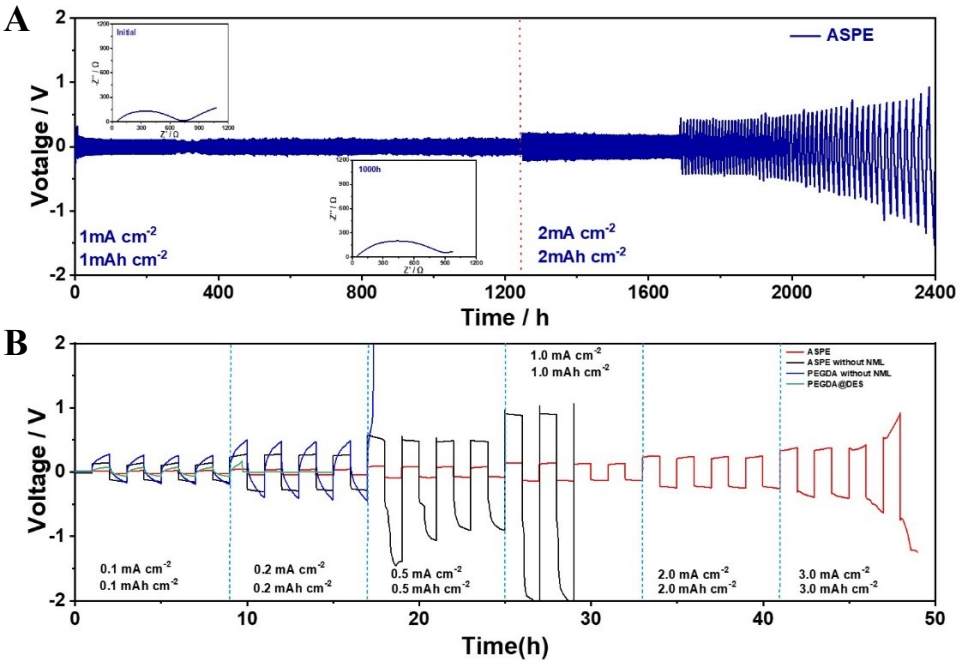

Fig. S17. (**A**) Voltage profile of the Li||Li symmetric cells using ASPE electrolyte at 1and 2 mA cm^{-2} with a cut-off capacity of 1 and 2 mAh cm^{-2}. At a high current density of 1mA cm^{-2}, Li|ASPE|Li symmetric cells can be cycled stably for more than 1250 hours, and the polarization voltage is about 200 mV. When the current density increases to 2mA cm^{-2}, the symmetrical cells can adapt to the current change, effectively, and can be cycled stably for about 500 hours. The above results show that ASPE electrolyte can effectively alleviate the safety problems caused by lithium dendrite under high current. (**B**) Plating and stripping curves of a symmetrical cell with different polymer electrolytes measured at room temperature.

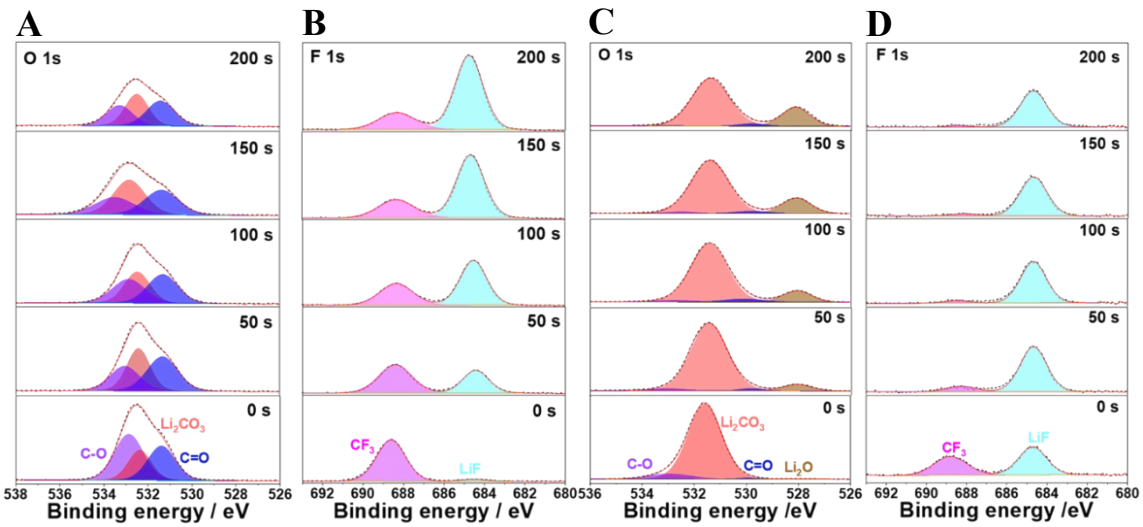

Fig. S18. (**A** and **C**) O 1s and （**B** and **D**) F 1s in-depth XPS spectra of Li metal anodes from Li symmetric cells using (**A** and **B**) ASPE and (**C** and **D**) PEGDA electrolytes after 40 cycles.

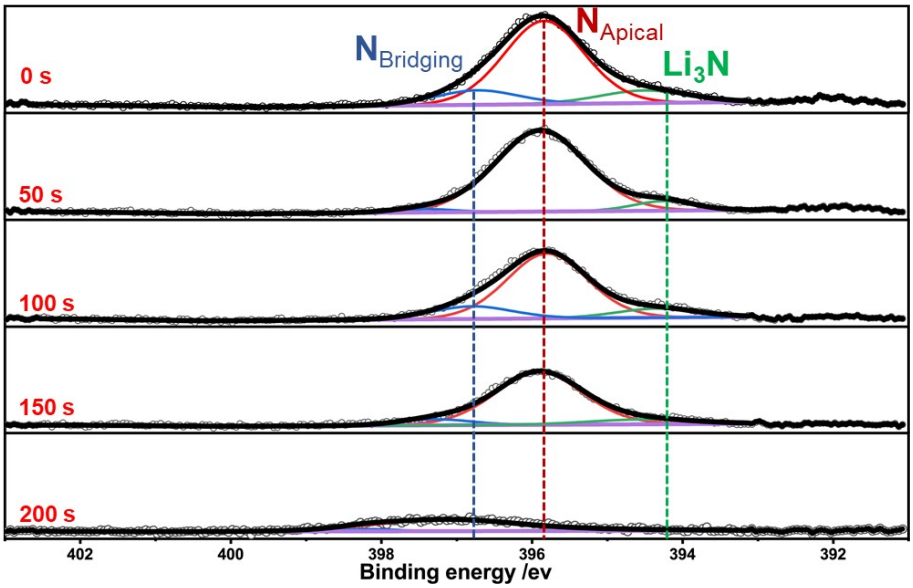

Fig. S19. **XPS analysis.** Chemical evolution of N 1s along Li/ASPE interphase by XPS depth profiling.

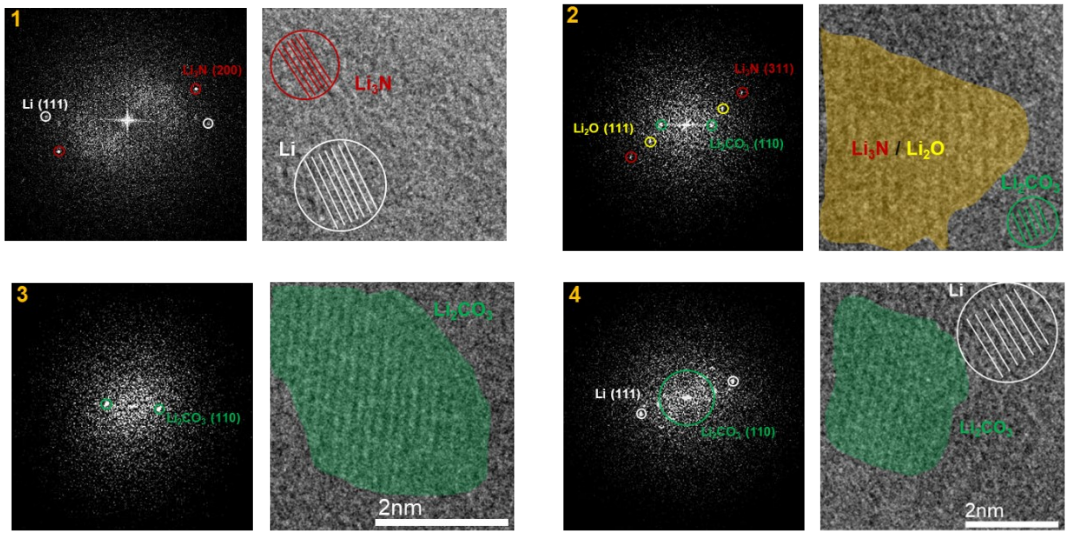

Fig. S20. FFT patterns corresponding to regions 1–4 as highlighted in **Fig. 4**(**I**), respectively. Nanostructure schematic overlaying the HRTEM images that correspond to regions 1–4 as highlighted in (Fig. 4 **I**), respectively.

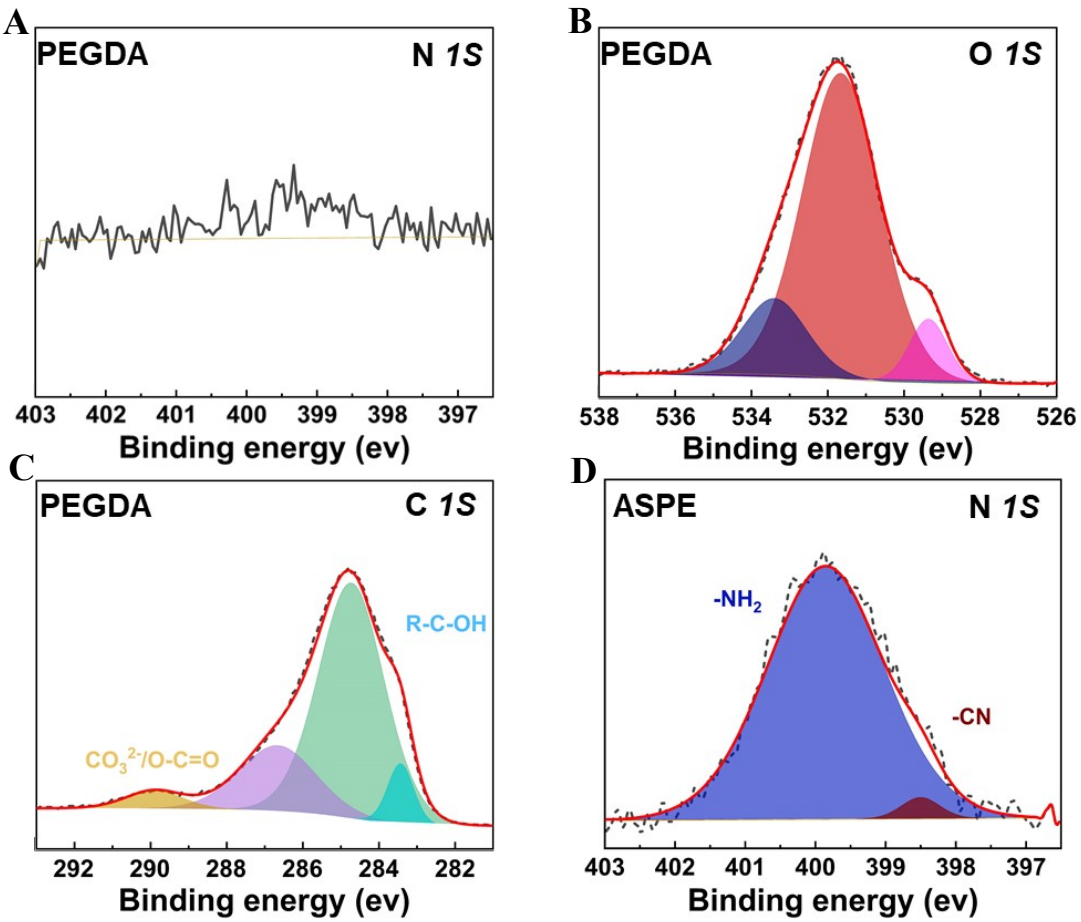

Fig. S21. **Chemical evolution of N 1s, O 1s and C 1s along SPEs/LCO interphase by XPS profiling.** (**A**-**C**) PEGDA and (**D**) ASPE electrolytes after 10 cycles.

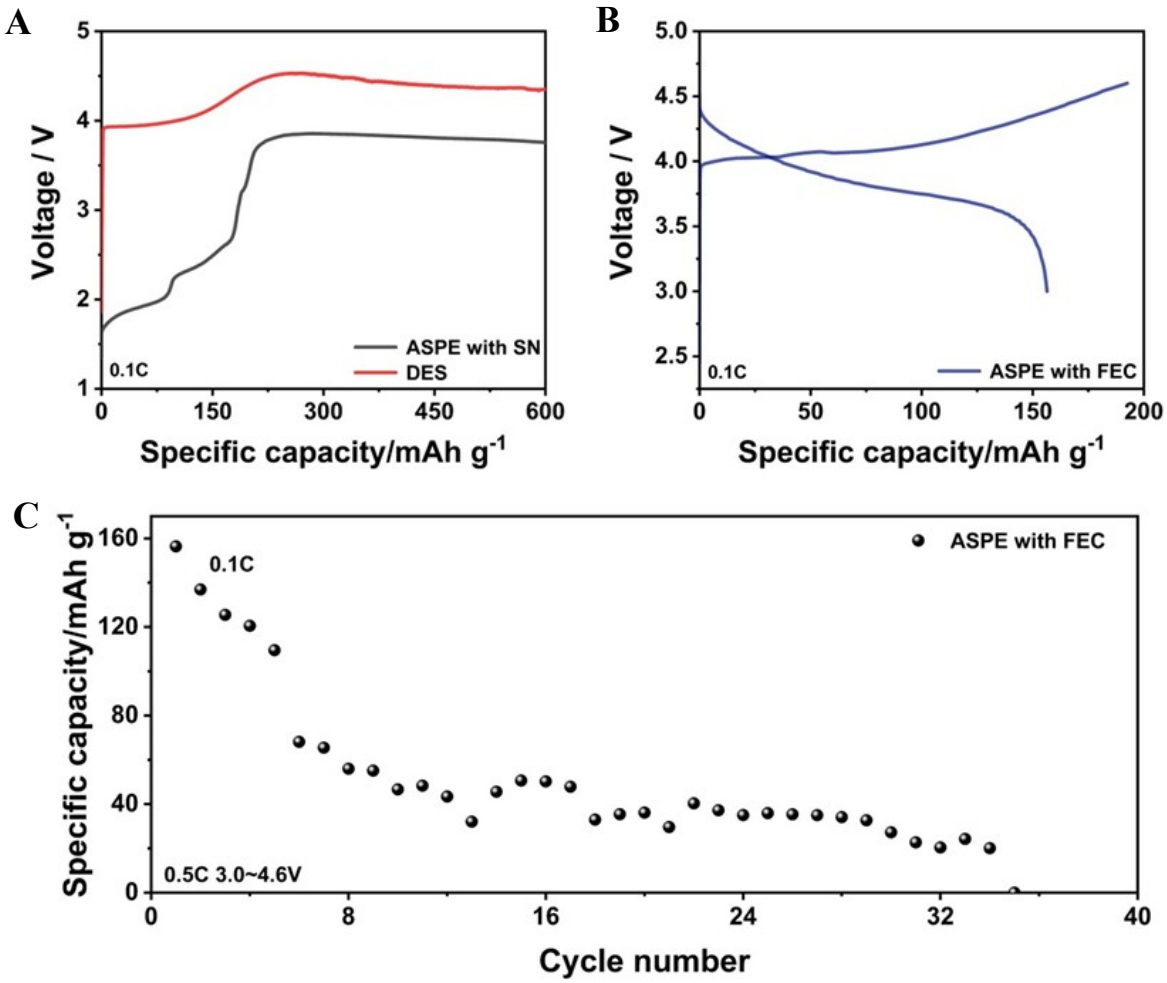

Fig. S22. (**A**) Charge profiles of the Li | DES | LCO and Li | ASPE with SN | LCO half cells at 0.1 C and room temperature. DES electrolyte and ASPE with SN electrolyte can't meet the charging and discharging requirements of high-voltage LCO, and the electrolytes will decompose before reaching 4.6V. (**B**) Discharge/charge profiles of the Li | ASPE with FEC | LCO half cells at 0.1 C and room temperature. (**C**) Cycle performance of Li | ASPE with FEC | LCO half cells.

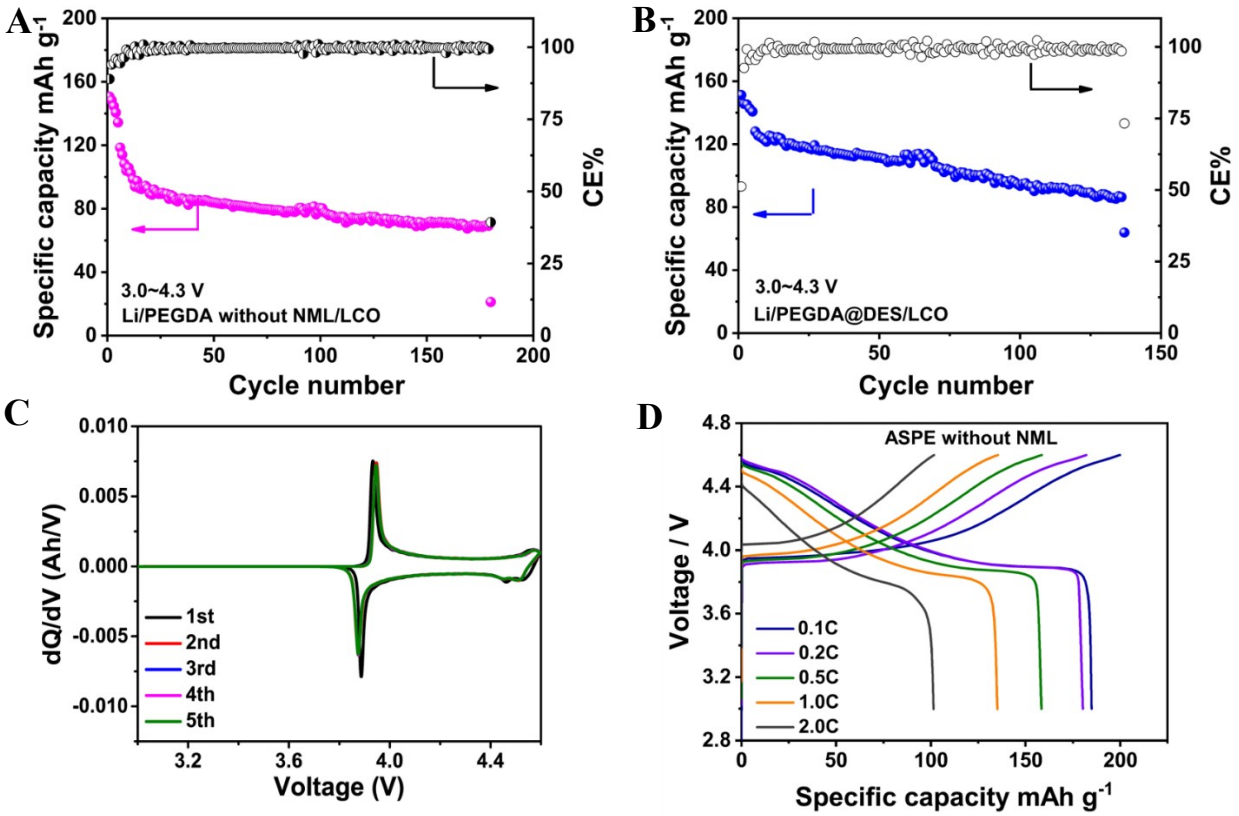

Fig. S23. Cycle performance of Li|PEGDA without NML|LCO (**A**) and Li|PEGDA @ DES|LCO (**B**) at 0.5 C and room temperature (0.1 C activation for the first 5 cycles). (**C**) dQ/dV curves of $LiCoO_2$/Li metal batteries with the electrolytes of ASPE. From the charging process, it can be observed that the peak voltage slightly increases in the first two cycles and in the subsequent cycles maintains stable. The voltage increase in the first two cycles is attributed to the oxidation of ASPE and formation of stable CEI, which is stable in subsequent cycles. The discharge processes are perfectly matched, and stable CEI as well. (**D**) Charge and discharge curves of Li|ASPE without NML|LCO at different C-rates.

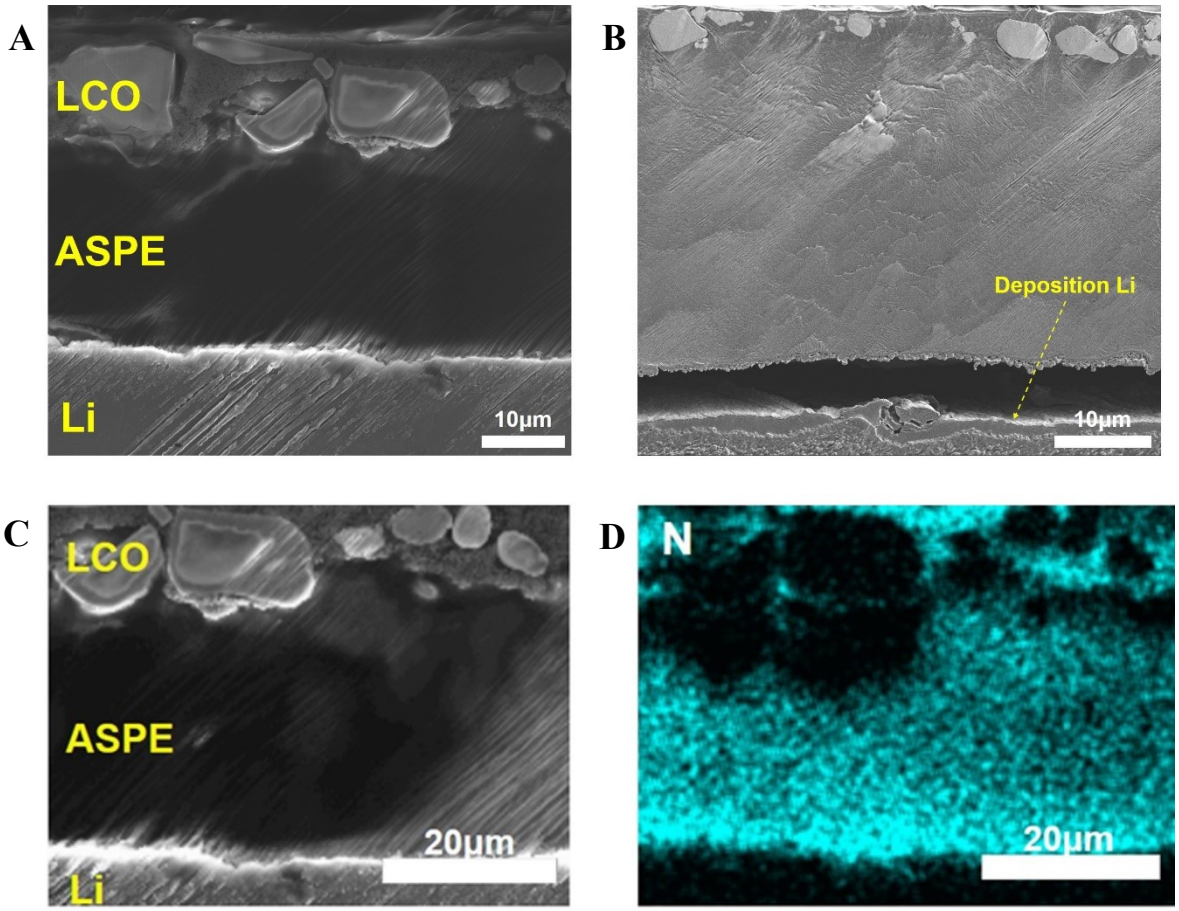

Fig. S24. (**A**) Cross-sectional SEM images of the Li | ASPE | LCO. (**B**) Using low-temperature "solid-solid separation technology" SEM of the Li | ASPE | LCO. It is obvious that after cycles, no Li dendrites are formed on the anode surface. (**C**) Cross-sectional mapped area of the half-cell and (**D**) N element distribution. The N element in NML is uniformly distributed in the ASPE and the cathode. This is because the polymer precursor liquid can effectively infiltrate the cathode and form a cathode-electrolyte network after in-situ polymerization.

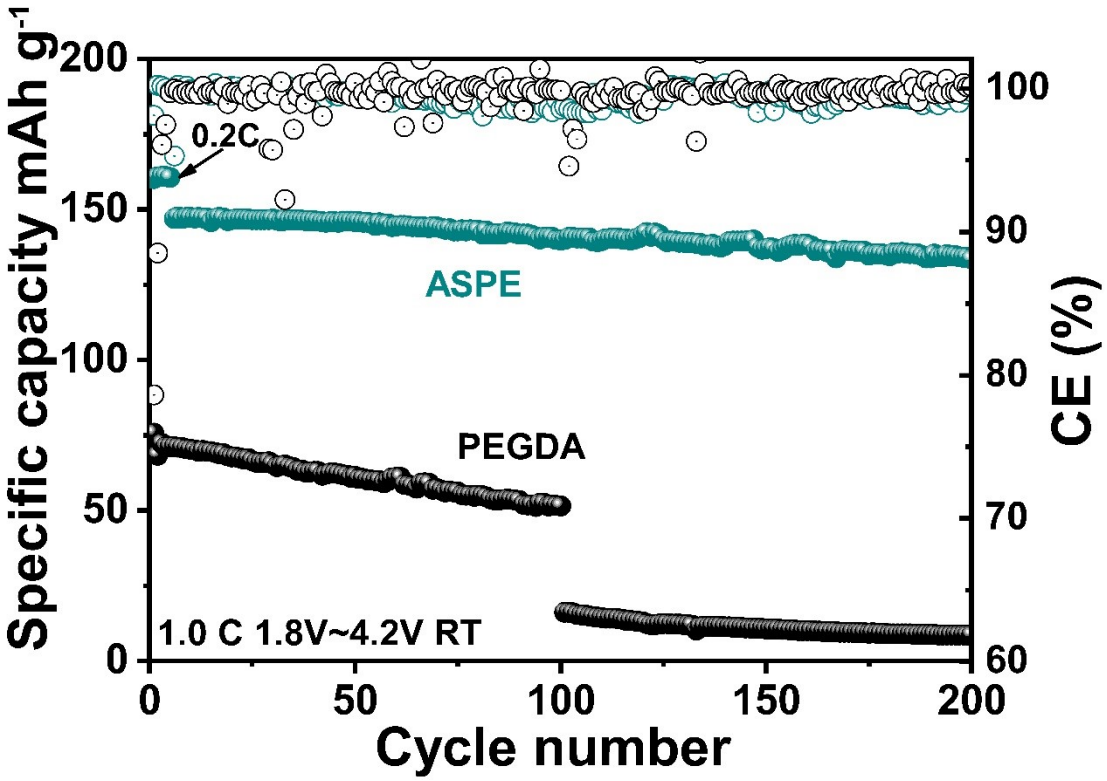

Fig. S25. Cycle performance of Li|SPEs|LFP.

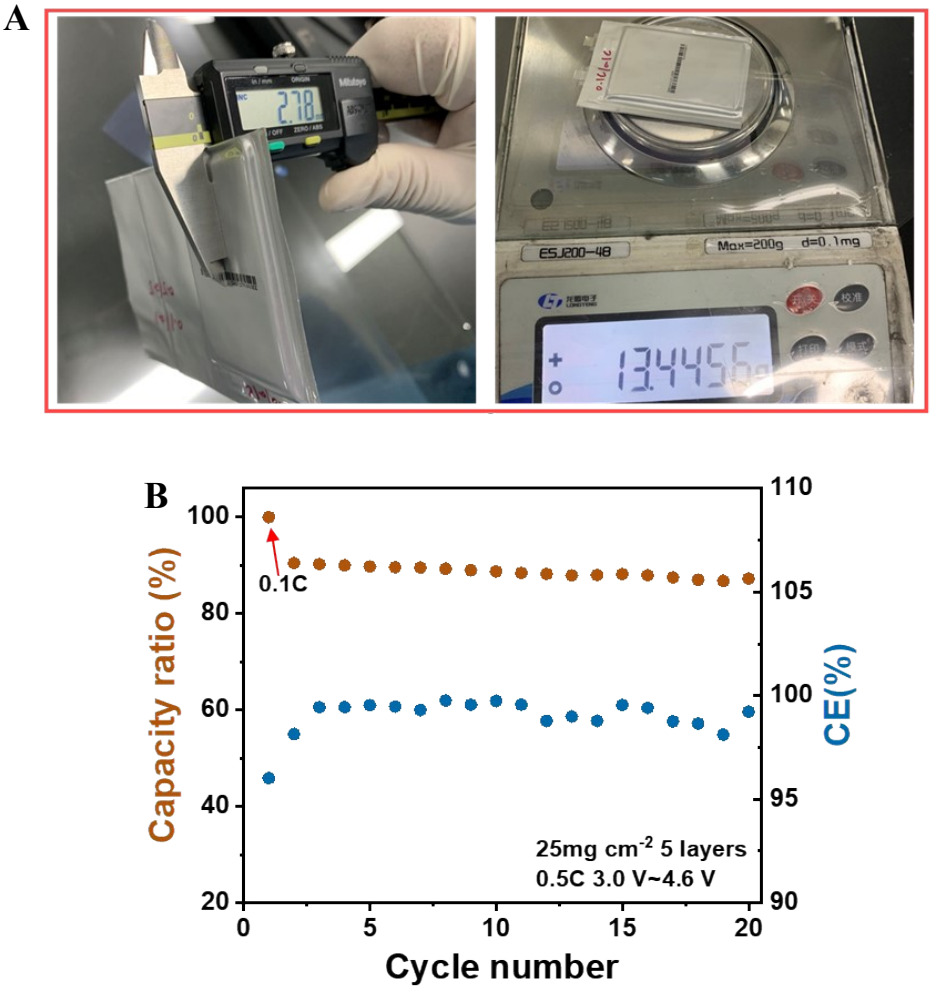

Fig. S26. (**A**) Optical image for the thickness and mass of the pouch cell. (**B**) pouch cell long cycle performance.

Table 1. Real parameters of the pouch cell with a specific energy of >425 Wh kg^{-1}.

Component of Cell	Parameter	Real Value
Cathode	Active Material Ratio (%)	97.2
	Areal Load (mg cm^{-2})	25
	Number of Cathode Sheet	5
Anode	Thickness(μm)	50 (10 Cu+2*20 Li)
Electrolyte	Injection Mass (g)	2.3
Cell	1th Discharge Capacity (mAh)	1402.8
	1th Discharge Energy (Wh)	5.7632
	Total Mass (g)	13.4456
	Thickness (mm)	2.78
	Energy Density (Wh kg^{-1})	428.63

Table 2. Performance comparison of different types of solid electrolytes at high voltage.

Type	Composition	Anode/ Cathode	VR (V)	Q (mAh g^{-1})	Rate	Cycle Life	Ref
Polymer	NML/LiTFSI/ PEGDA/UPyMA	Li/LCO	3.0~4.6	188.5	0.5C	1000	This work
Polymer	PEGDA/BA/SN/LiTFSI	Li/NMC-83	2.7~4.5	190	0.2 mA cm^{-2}	_	[2]
Polymer	PEO-LiDFOB-SN	Li/LCO	2.5~4.45	144.5	0.1C	50	[3]
Polymer	PFEC/LiDFOB / cellulose separator	Li/LCO	3.0~4.45	162	0.1C	50	[4]
Polymer	PEO/SN/LiTFSI/LiTFPFB/	Li/LCO	2.5~4.3	150	0.1C	100	[5]
Ceramic oxide	LLTO	Li/LFP	2.8~4.0	145	0.1C	100	[6]
Ceramic oxide	LCBO/LLZO	Li/LCO	3.0~4.1	~83	0.05	100	[7]
Ceramic oxide	LLCZN/ 1 M $LiPF_6$ in FEC/FEMC/HFE	Li/LFMO	3.5~5.3	103	0.1	50	[8]
Ceramic oxide	Cu_3N-LLZTO	Li/LCO	3.2~4.25	~125	0.2	300	[9]
Composite	LLZTO/PVDF-HFP/ liquid electrolyte	Li/NMC622	2.8~4.5	194	0.1C	50	[10]
Composite	LLZTO/ TPGDA /$VEImNTF_2$	Li/LFP	2.8~3.8	149.3	0.5C	300	[11]
Composite	PAN-LAGP-PEGDA	Li/NMC811	2.8~4.3	175	0.5	~100	[12]
Composite	PEGDA/PETMP/MOF	Li/LCO	3.0~4.5	136	0.5	100	[13]
Composite	PEO–LiClO4–LLZTO	Li/LCO	2.7~4.2	~110	0.4C	1000	[14]

Nomenclature: VR: Voltage range; Q: specific capacity; BA: butyl acrylate; SN: succinonitrile; PFEC: Poly(fluoroethylene carbonate); CS: cellulose separator; LLTO: $Li_{0.34}La_{0.56}TiO_3$; NMC-83: $LiNi_{0.83}Mn_{0.06}Co_{0.11}O_2$; LLZO: Li7La3Zr2O12; LAGP: $Li_{1.5}Al_{0.5}Ge_{1.5}P_3O_{12}$; LLCZN: $Li_7La_{2.75}Ca_{0.25}Zr_{1.75}Nb_{0.25}O_{12}$; LFMO: $Li_2FeMn_3O_8$; LLZTO: $Li_{6.4}La_3Zr_{1.4}Ta_{0.6}O_{12}$; TPGDA: tripropylene glycol diacrylate; $VEImNTF_2$: 1-vinyl-3-ethylimidazolium bis(trifluoroethylimidazolium sulfonyl)imide; PETMP: tetrakis (3-mercaptopropionic acid) pentaerythritol.

Table 3. Performance comparison of different types of solid electrolytes with Li-rich Mn cathode.

Ref	Type	Composition	Anode/ Cathode	Comp. (wt%)	Loading (mg cm^{-2})	VR (V)	Q (mA $h\ g^{-1}$)	Rate (C)
This work	Polymer	NML/LiTFSI/ PEGDA/UPyMA	Li/LNCM	75:10:10: 5	2.5	2.1~ 4.9	246	0.2
[15]	Gel	3 wt% DAP/1.5 wt% PETEA/1.0 M $LiPF_6$-FEC-FEMC-HTE	Li/LRO	80:10:10	3	2.0~ 5.0	191. 1	0.2
[16]	Gel	PVDF-HFP/CA/SN/ ZIF-8/PEO/Al_2O_3/1.0 M $LiPF_6$-EC/DMC	Li/LLO	80:10:10	2.5	2.0~ 4.8	257. 5	0.2

Nomenclature: Comp: composition of cathode (active material : binder : electrical conductive additive : solid electrolyte); VR: Voltage range; Q: specific capacity; NML: N-methylurea; PEGDA: polyethylene glycol diacrylate; UpyMA: 2-(3-(6-methyl-4-oxo-1,4-dihydropyrimidin-2-yl) ureido) ethyl methacrylate; LNCM: $Li_{1.2}Ni_{0.13}Co_{0.13}Mn_{0.54}O_2$; DAP: diethyl allyl phosphate; PETEA: pentaerythritol tetraacrylate; FEC: fluoroethylene carbonate; FEMC: 2,2,2-trifluoroethylmethyl carbonate; THE: 1,1,2,3,3,3-hexafluoropropyl-2,2,2-trifluoroethylether; LRO: $Li_{1.2}Mn_{0.54}Ni_{0.13}Co_{0.13}O_2$; CA: cellulose acetate; SN: succinonitrile; LLO: $Li_{1.2}Ni_{0.13}Co_{0.13}Mn_{0.54}O_2$.It should be mentioned that the study of the Li-rich Mn-cathode with solid-state polymer electrolyte has not been reported, and the Li-rich Mn-cathode with quasi-solid-state polymer electrolyte has been reported in a few.

References

1. B. Zhou, D. He, J. Hu, Y. Ye, H. Peng, X. Zhou, X. Xie and Z. Xue, *Journal of Materials Chemistry A*, 2018, **6**, 11725-11733.
2. M. J. Lee, J. Han, K. Lee, Y. J. Lee, B. G. Kim, K.-N. Jung, B. J. Kim and S. W. Lee, *Nature*, 2022, **601**, 217-222.
3. J. Ma, Z. Liu, B. Chen, L. Wang, L. Yue, H. Liu, J. Zhang, Z. Liu and G. Cui, *Journal of The Electrochemical Society*, 2017, **164**, A3454-A3461.
4. J. Liu, X. Shen, J. Zhou, M. Wang, C. Niu, T. Qian and C. Yan, *ACS Applied Materials & Interfaces*, 2019, **11**, 45048-45056.
5. C. Wang, T. Wang, L. Wang, Z. Hu, Z. Cui, J. Li, S. Dong, X. Zhou and G. Cui, *Advanced Science*, 2019, **6**, 1901036.
6. Z. Jiang, S. Wang, X. Chen, W. Yang, X. Yao, X. Hu, Q. Han and H. Wang, *Adv. Mater.*, 2020, **32**, 1906221.
7. F. Han, J. Yue, C. Chen, N. Zhao, X. Fan, Z. Ma, T. Gao, F. Wang, X. Guo and C. Wang, *Joule*, 2018, **2**, 497-508.
8. X. Han, Y. Gong, K. Fu, X. He, G. T. Hitz, J. Dai, A. Pearse, B. Liu, H. Wang, G. Rubloff, Y. Mo, V. Thangadurai, E. D. Wachsman and L. Hu, *Nature Materials*, 2017, **16**, 572-579.
9. H. Huo, Y. Chen, R. Li, N. Zhao, J. Luo, J. G. Pereira da Silva, R. Mücke, P. Kaghazchi, X. Guo and X. Sun, *Energy & Environmental Science*, 2020, **13**, 127-134.
10. X. Li, L. Cong, S. Ma, S. Shi, Y. Li, S. Li, S. Chen, C. Zheng, L. Sun, Y. Liu and H. Xie, *Advanced Functional Materials*, 2021, **31**, 2010611.
11. J. Li, Y. Cai, Y. Cui, H. Wu, H. Da, Y. Yang, H. Zhang and S. Zhang, *Nano Energy*, 2022, **95**, 107027.
12. H. Duan, M. Fan, W.-P. Chen, J.-Y. Li, P.-F. Wang, W.-P. Wang, J.-L. Shi, Y.-X. Yin, L.-J. Wan and Y.-G. Guo, *Adv. Mater.*, 2019, **31**, 1807789.
13. H. Wang, Q. Wang, X. Cao, Y. He, K. Wu, J. Yang, H. Zhou, W. Liu and X. Sun, *Adv. Mater.*, 2020, **32**, 2001259.
14. J. Liang, D. Chen, K. Adair, Q. Sun, N. G. Holmes, Y. Zhao, Y. Sun, J. Luo, R. Li, L. Zhang, S. Zhao, S. Lu, H. Huang, X. Zhang, C. V. Singh and X. Sun, *Advanced Energy Materials*, 2021, **11**, 2002455.
15. J. Wu, X. Wang, Q. Liu, S. Wang, D. Zhou, F. Kang, D. Shanmukaraj, M. Armand, T. Rojo, B. Li and G. Wang, *Nature Communications*, 2021, **12**.
16. S. Cui, X. Wu, Y. Yang, M. Fei, S. Liu, G. Li and X.-P. Gao, *ACS Energy Letters*, 2022, **7**, 42-52.